THERMODYNAMICS AND MOLECULAR-SCALE PHENOMENA

Structural insights into peptide self-assembly using photo-induced crosslinking experiments and discontinuous molecular dynamics

Samuel J. Bunce[1,2] | Yiming Wang[3,4] (ORCID) | Sheena E. Radford[2,5] |
Andrew J. Wilson[1,2] (ORCID) | Carol K. Hall[3]

[1]School of Chemistry, University of Leeds, Leeds, UK

[2]Astbury Centre for Structural Molecular Biology, University of Leeds, Leeds, UK

[3]Department of Chemical and Biomolecular Engineering, North Carolina State University, Raleigh, North Carolina

[4]Department of Chemical and Biological Engineering, Princeton University, Princeton, New Jersey

[5]School of Molecular and Cellular Biology, University of Leeds, Leeds, UK

Correspondence
Carol K. Hall, Department of Chemical and Biomolecular Engineering, North Carolina State University, Raleigh, NC 27695-7905.
Email: hall@ncsu.edu

Funding information
Biotechnology and Biological Sciences Research Council, Grant/Award Number: BB/J014443/1; Engineering and Physical Sciences Research Council, Grant/Award Numbers: EP/KO39292/1, EP/N013573/1, EP/N035267/1; NSF Division of Chemical, Bioengineering, Environmental, and Transport Systems, Grant/Award Numbers: 1512059, 1743432; Royal Society Leverhulme Trust Senior Fellowship, Grant/Award Number: SRF/R1/191087; Wellcome Trust, Grant/Award Numbers: 090932/Z/09/Z, 094232/Z/10/Z

Abstract

Determining the structure of the (oligomeric) intermediates that form during the self-assembly of amyloidogenic peptides is challenging because of their heterogeneous and dynamic nature. Thus, there is need for methodology to analyze the underlying molecular structure of these transient species. In this work, a combination of fluorescence quenching, photo-induced crosslinking (PIC) and molecular dynamics simulation was used to study the assembly of a synthetic amyloid-forming peptide, $A\beta_{16-22}$. A PIC amino acid containing a trifluormethyldiazirine (TFMD) group—Fmoc (TFMD)Phe—was incorporated into the sequence ($A\beta^*_{16-22}$). Electrospray ionization ion-mobility spectrometry mass-spectrometry (ESI-IMS-MS) analysis of the PIC products confirmed that $A\beta^*_{16-22}$ forms assemblies with the monomers arranged as anti-parallel, in-register β-strands at all time points during the aggregation assay. The assembly process was also monitored separately using fluorescence quenching to profile the fibril assembly reaction. The molecular picture resulting from discontinuous molecule dynamics simulations showed that $A\beta_{16-22}$ assembles through a single-step nucleation into a β-sheet fibril in agreement with these experimental observations. This study provides detailed structural insights into the $A\beta_{16-22}$ self-assembly processes, paving the way to explore the self-assembly mechanism of larger, more complex peptides, including those whose aggregation is responsible for human disease.

KEYWORDS
amyloid-forming peptide, discontinuous molecular dynamics, peptide self assembly, photo-induced crosslinking

1 | INTRODUCTION

Self-assembling peptides can be difficult to study in vitro because of their hydrophobicity and propensity to aggregate into high order

assemblies.[1-4] Consequently, shorter synthetic peptide fragments from longer amyloidogenic sequences offer convenient model systems with which to explore peptide self-assembly.[5,6] A case in point is the Gly-Asn-Asn-Gln-Gln-Asn-Tyr (GNNQQNY) sequence, taken from the prion-determining domain (PrD) of the 635 residue Sup35 yeast protein.[7,8] Eisenberg and co-workers established in 2001 that in aqueous conditions this sequence self-assembles into highly ordered fibril structures that display the characteristic cross-β X-ray diffraction pattern of amyloid.[6] The short nature of GNNQQNY enabled the formation of micro-crystals suitable for electron diffraction, which demonstrated that in the crystals the peptide had formed a parallel in-register β-sheet structure involving a steric zipper with a dry interface between the interdigitated side-chains.[7] GNNQQNY clearly demonstrates that peptide fragments can be useful models of longer amyloid sequences, revealing atomic level information about short segments that may be relevant to the assembly of their longer peptide counterparts.

One of the most widely studied short amyloidogenic sequences is Aβ$_{16-22}$ (Ac-Lys-Leu-Val-Phe-Phe-Ala-Glu-CONH$_2$), a seven-residue peptide that comes from the central fibril-forming region of the Aβ sequence associated with Alzheimer's disease.[5] Aβ$_{16-22}$ is one of the smallest Aβ fragments that forms fibrils with a cross-β structure and can be readily synthesized using solid phase peptide synthesis (SPPS). Substitutions within this region of full-length Aβ peptide have been shown to affect its aggregation propensity in vitro and in vivo, highlighting the importance of the motif.[9-11] These findings make Aβ$_{16-22}$ a convenient model with which to explore the underlying steps in an aggregation mechanism. The noted ability of Aβ$_{16-22}$ to form a range of supramolecular structures at different pH values further highlights the value of using Aβ$_{16-22}$ to understand the fundamental molecular mechanisms of peptide self-assembly and the molecular origins of fibril polymorphism.[12,13] Tycko and co-workers used solid-state NMR, transmission electron microscopy (TEM) and X-ray diffraction to establish that at neutral pH Aβ$_{16-22}$ formed in-register, anti-parallel fibril structures that displayed green birefringence when bound to Congo-Red.[5] In X-ray diffraction experiments the fibrils displayed periodic reflections at 4.9 and 9.9 Å, characteristic of the spacing between β-strands and β-sheet layers, respectively.[14,15]

A key goal in studying Aβ$_{16-22}$ is to understand the transitions that occur during self-assembly. Petty and Decatur used isotope-edited IR to establish that at neutral pH, Aβ$_{16-22}$ assembles with monomers adopting an initial β-strand alignment that is not identical to the final equilibrium alignment, that is, there is some β-sheet reorganization during the self-assembly process.[16] Lynn and co-workers demonstrated that at both acidic and neutral pH, Aβ$_{16-22}$ passes through an intermediary out-of-register ribbon-like structure.[13] The time taken to reach the final fibril alignment (measured by CD) was different at each pH: at neutral pH Aβ$_{16-22}$ reached a plateau after 5 days, whereas at acidic pH a lag phase of 4 days was observed, with the final plateau being reached after 10 days.[13] Aβ$_{16-22}$ has also been shown to form micrometer sized particles with a high concentration of peptides in a liquid-like state.[17,18] These particles are metastable (containing around 20–33% β-sheet content) and can undergo a phase transition to form nanotubes or fibrils at certain temperatures and pH

values. In all cases, it should be noted that changes in temperature, peptide concentration and ionic strength can have a significant impact on the kinetics of Aβ$_{16-22}$ aggregation, confounding comparison between different studies.[12,13,18,19]

Since the transient intermediates that form during the early stages of peptide self-assembly can be difficult to characterize experimentally, molecular dynamics (MD) simulations can provide useful insights.[20-22] The first studies, carried out by Klimov and Thirumalai, demonstrated that monomeric Aβ$_{16-22}$ preferentially adopts either a random coil or extended β-sheet conformation.[20] These structures then progress through an obligatory α-helical intermediate prior to forming stable anti-parallel, in-register oligomers. Later studies also observed that Aβ$_{16-22}$ monomers adopt primarily random coil conformations, although the presence of an α-helical intermediate was disputed.[21,22] These simulations also highlighted the complex pathways that Aβ$_{16-22}$ accesses during the self-assembly process and that the anti-parallel, in-register structure is the preferred structure due to its stability. Hall and co-workers[23] applied discontinuous molecular dynamics (DMD) and a coarse-grained protein model (PRIME20) to demonstrate that at high simulation temperatures, a system of 48 monomeric Aβ$_{16-22}$ peptides aggregates via classical nucleation and growth into a highly-ordered structure with monomers organized as anti-parallel, in-register β-strands in agreement with the solid-state NMR measurements reported by Tycko and co-workers.[5] At lower simulation temperatures, Aβ$_{16-22}$ first forms β-sheet-rich oligomers which then merge and rearrange into a large fibril. Later, Hall and co-workers[24] combined the DMD/PRIME20 simulation with classical nucleation theory to construct a thermodynamic (solubility) phase diagram for Aβ$_{16-22}$, which agrees well with in vitro solubility measurements. Recently, PRIME20/DMD simulations were combined with electrospray ionization ion-mobility spectrometry mass-spectrometry (ESI-IMS-MS) measurements to reveal structural insights on the secondary nucleation mechanism of Aβ$_{1-40}$ peptide on Aβ$_{16-22}$ fibril surface.[25]

In this work, we combine experimental and molecular simulation to understand and characterize, at the molecular level, the transitions that Aβ$_{16-22}$ undergoes as it self-assembles. We used photo-induced crosslinking (PIC) combined with ESI-IMS-MS to derive insights on the noncovalent organization of Aβ$_{16-22}$ during different phases of its self-assembly reaction. The simulation results are in close agreement with experimental results, and indicate that the dominant pathway by which Aβ$_{16-22}$ assembles involves monomers organized as anti-parallel, in-register β-strands at all time points. The results highlight the power of combining PIC with ESI-IMS-MS/MS, fluorescence quenching and DMD simulations to study kinetic intermediates in peptide self-assembly, and paves the way for exploring the self-assembly of larger, more complex peptides, including those directly relevant to amyloid disease.

2 | MATERIALS AND METHODS

2.1 | Solid Phase Peptide Synthesis of Aβ$_{16-22}$

All amino acids, 4-(trifluormethyldiazirine)phenylalanine (TFMD-Phe), Aβ$_{16-22}$ (Ac-Lys-Leu-Val-Phe-Phe-Ala-Glu-NH$_2$), Aβ$_{16-22}$ N-terminally

labeled with tetramethylrhodamine (TAMRA) including a 6-aminohexanoic acid linker (Ahx); TAMRA-Ahx-Aβ$_{16-22}$ and Aβ$_{16-22}$ functionalized TFMD-Phe; Aβ*$_{16-22}$ (Ac-Lys-Leu-Val-Phe-(TFMD)Phe-Ala-Glu-NH$_2$) were prepared as described previously.[25-27]

2.2 | Fluorescence quenching assays

Fluorescence quenching assays were carried out as described previously.[25] Briefly Aβ$_{16-22}$ was spiked with 5% (w/w) TAMRA-Ahx-Aβ$_{16-22}$ (total peptide concentration, 20 or 40 μM) in 100 mM ammonium bicarbonate buffer (pH 7.4) with a final concentration of 2% (v/v) DMSO. Samples were placed in quartz cuvettes and analyzed using a temperature-controlled fluorimeter at 37°C. Time points were taken every 30 s for the duration of the experiment. The TAMRA fluorophore was excited at 520 nm, and emission was recorded at 600 nm to reduce the inner filter effect.

2.3 | TEM analyses

Samples were prepared and analyzed by TEM as described previously.[25] Briefly, TEM images were taken at the stated time points and at the end of each experiment by removing 5 μl from the assembly reaction and incubating this sample on carbon–formvar grids for 30 s before staining with 2% (w/v) uranyl acetate solution for an additional 30 s. Images were taken on a JEM-1400 (JEOL Ltd., Tokyo, Japan) or a Tecnai F12 TEM. (FEI, Hillsboro, OR) TEM. Images were taken using either an ATM charge-coupled device (CCD) camera or a Gatan UltraScan 1,000 XP (994) CCD camera (JEM-1400) or an UltraScan 100XP (994) CCD camera (Tecnai F12). Once taken, images were processed using ImageJ (National Institutes of Health [NIH]).

2.4 | Photo-induced cross-linking

Aβ*$_{16-22}$ (40 μM total peptide concentration) in 100 mM ammonium bicarbonate buffer (pH 7.4) with a final concentration of 1% (v/v) DMSO was incubated quiescently in Eppendorf tubes for 0 min, 5 min, or 24 hr. Samples were then irradiated for 30 s using a light-emitting diode lamp at 365 nm,[28] then removed, lyophilized overnight, redissolved in hexafluorisopropanol (HFIP) for at least 2 hr, and vortexed to ensure disaggregation. HFIP was then removed under a stream of N$_2$, and the sample was re-suspended in 50:50 (v/v) MeCN/H$_2$O containing 0.05% (v/v) formic acid to a final peptide concentration of ∼40 μM. Cross-links were then analyzed using ESI-IMS-MS/MS as described below.

2.5 | Electrospray ionization ion-mobility spectrometry mass-spectrometry (ESI-IMS-MS/MS)

All samples were prepared as described above and left to incubate at 37°C without agitation for 5 min. A SYNAPT HDMS quadrupole time-of-flight MS (Micromass UK Ltd., Waters Corp., Manchester, UK), equipped with a TriVersa NanoMate (Advion Biosciences, Ithaca, NY) automated nano-ESI interface was used in this study. The instrument has a traveling-wave IMS device situated in between the quadrupole and the time-of-flight analyzer. Samples were analyzed by positive ionization nano-ESI, with a capillary voltage of 1.4 kV and a nitrogen-nebulizing gas pressure of 0.8 psi. The following instrumental parameters were set: cone voltage, 60 V; source temperature, 60°C; backing pressure, 4.7 mbar; ramped traveling speed, 7 to 20 V; traveling wave speed, 400 m s^{-1}; IMS nitrogen gas flow, 20 ml min^{-1}; IMS cell pressure, 0.55 mbar. The mass/charge ratio (m/z) scale was calibrated using aq. CsI cluster ions. Collision Cross Section (CCS) measurements were estimated using a calibration obtained by analysis of denatured proteins (cytochrome c, ubiquitin, and alcohol dehydrogenase) and peptides (tryptic digests of alcohol dehydrogenase and cytochrome c), with known CCSs obtained elsewhere from drift tube ion mobility measurements.[29,30] The CCS (Ω) of the peptide monomers/oligomers was then calculated according to Equation (1):

$$\Omega\left(°A^2\right) = A \times (t_D)^B \times z \times \sqrt{\frac{1}{m_{ion}} + \frac{1}{m_{gas}}} \tag{1}$$

where A is the determined calibration constant, z is the charge state of the ion, B is the exponential factor (determined experimentally), t_D is the corrected absolute drift time, m_{ion} is the mass of the ion and m_{gas} is the mass of the gas used in the ion-mobility cell (N$_2$). Data were processed using MassLynx v4.1 and Driftscope software supplied with a mass spectrometer.

2.6 | DMD simulation

In this work, three independent DMD/PRIME20 simulations were carried out for 12 μs in the canonical (NVT) ensemble. The two major nonbonded interactions of the PRIME20 model are the directional square-well backbone hydrogen bonding interaction and the nondirectional square-well potential interaction between two sidechain beads. The potential energy parameters between the 20 different amino acids include 210 independent square-well widths and 19 independent square-well depths derived by using a perceptron learning algorithm that optimizes the energy gap between 711 known native states from the Protein Data Bank and decoy structures.[31] The Andersen thermostat was implemented to maintain the simulation system at a constant temperature.[32] One hundred and ninety-two peptides were initially randomly placed in a cubic box with a length of 321.0 Å, corresponding to a peptide concentration of 10 mM. The reduced temperature is defined to be $T^* = k_BT/\varepsilon_{HB}$, where ε_{HB} = 12.47 kJ/mol is the hydrogen bonding energy. The reduced temperature T^* of the simulations was set to be 0.193, which corresponds to 326 K in real temperature units.[33]

3 | RESULTS AND DISCUSSIONS

3.1 | Time course of Aβ16-22 aggregation

To monitor the time course for Aβ16-22 aggregation, we used a fluorescence quenching assay (Figure 1) in which sub-stoichiometric addition of a fluorescently labeled peptide, Aβ16-22 N-terminally labeled with tetramethylrhodamine (TAMRA) including a 6-aminohexanoic acid linker (Ahx); TAMRA-Ahx-Aβ16-22, was included in the Aβ16-22 assembly reaction (Aβ16-22/5% (w/w) TAMRA-Ahx-Aβ16-22 total peptide concentration, 20 or 40 μM). This assay, which is first used to study the aggregation of Aβ40 and Aβ42,[34] operates on the principle that fluorophores in adjacent peptides in an aggregated state are proximal and therefore self-quench. We used this assay in our previous study on secondary nucleation of Aβ40 by Aβ16-22.[25] Here, two different concentrations of Aβ16-22 were tested (20 and 40 μM); both self-assembly reactions (Figure 1a,b) proceed with a rapid initial decrease in fluorescence intensity followed by a second, slower, phase that reaches a plateau after around 1 hr.

Although a powerful method with which to measure the kinetics of peptide self-association in amyloid formation, fluorescence quenching is limited in that it reports only on the proximity of the fluorophores, but does not provide any information about the underlying structure(s) formed. To further understand the aggregation process of Aβ16-22, samples were taken during the aggregation time course after 5 min, 1 hr, and 24 hr, and analyzed by TEM (Figure 1c). At 5 min fibrils were observed with a small amount of amorphous aggregates also present. After a 1 hr incubation at 37°C, no
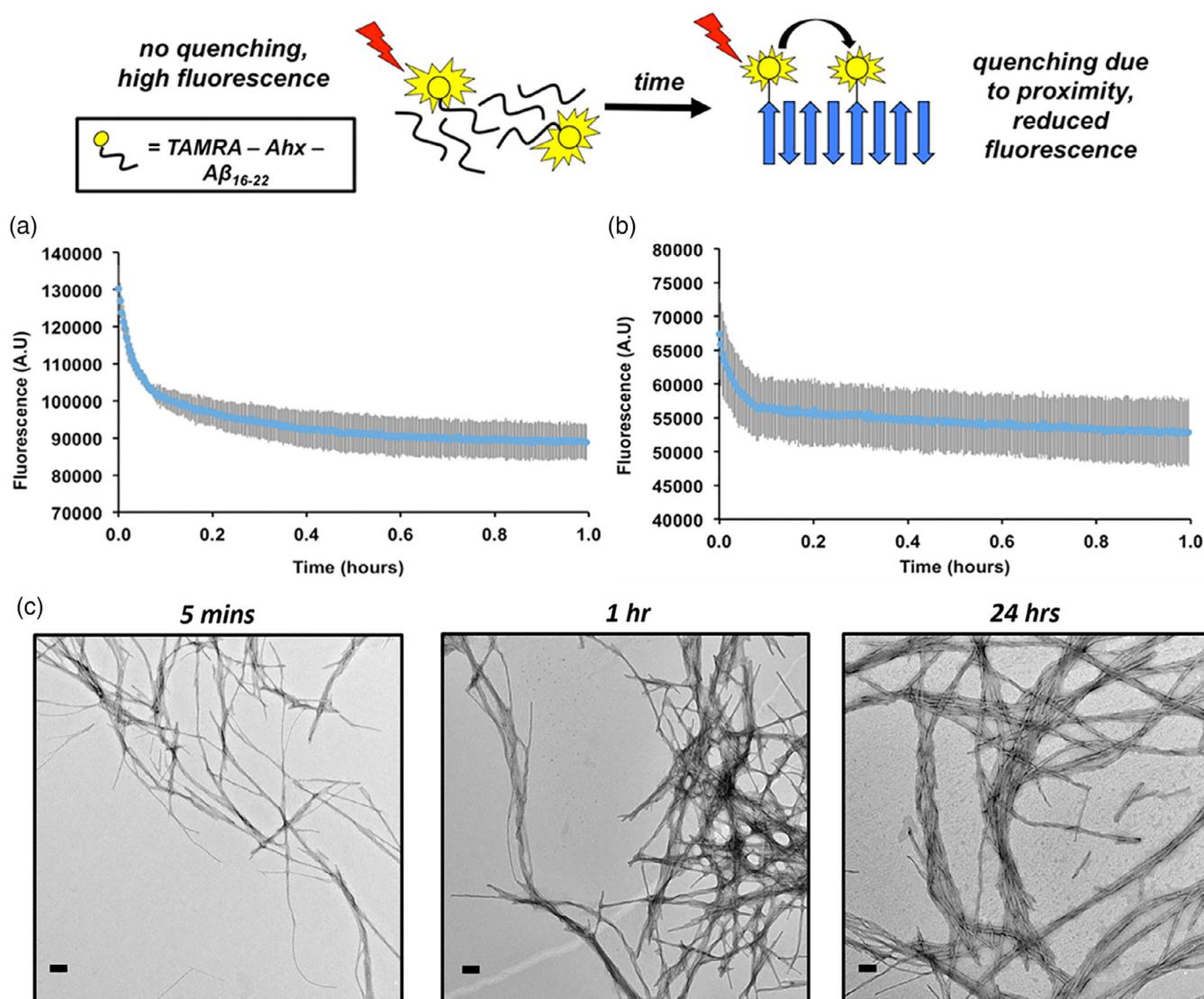
FIGURE 1 Schematic of the fluorescence quenching assay used in this work. As TAMRA-Ahx-Aβ16-22 is incorporated into the fibrils the fluorophores come into close contact and fluorescence is quenched. The aggregation kinetics of Aβ16-22 is monitored using fluorescence quenching. At both 40 and 20 μM (a and b, respectively), Aβ16-22 displays two-phase aggregation kinetics with the quenching reaching a plateau after around 1 h (100 mM ammonium bicarbonate buffer pH 7.4 with a final concentration of 2% (v/v) DMSO). In a TEM time course (c), Aβ16-22 (40 μM) forms highly ordered fibril structures within 5 min. Scale bar = 200 nm [Color figure can be viewed at wileyonlinelibrary.com]

amorphous aggregates could be seen and increased numbers of fibrils were observed on the grids. At these early time points, the fibrils were well dispersed without significant bundling, whereas at later time points (e.g., after 24 hr) significant bundling of the $A\beta_{16-22}$ fibrils was observed. The results show that under the conditions employed in this study, $A\beta_{16-22}$ forms fibril structures rapidly (within ~5 min), with increased numbers of fibrils formed at later times bundling together as the self-assembly reaction proceeds.

3.2 | Using ESI-IMS-MS and PIC to monitor structures formed during $A\beta_{16-22}$ aggregation

After establishing the aggregation kinetics of $A\beta_{16-22}$, the next step was to probe the structure(s) that $A\beta_{16-22}$ accesses during its transition from a monomer to a highly ordered β-sheet lattice within amyloid-like fibrils. This was achieved using $A\beta_{16-22}$ functionalized with 4-(trifluormethyldiazirine)phenylalanine (TFMD)Phe (named herein as $A\beta^*_{16-22}$). The requisite amino acid (TFMD-Phe) and peptide labeled with (TFMD)Phe at position 20 ($A\beta^*_{16-22}$, Figure 2) were prepared as described previously (Section 2).[25,26] Importantly, we have shown previously that the incorporation of (TFMD)Phe at positions 19 and 20 in $A\beta_{16-22}$ does not impede aggregation of the peptide nor, in the case of the F20 variant, does it alter the structure of the fibrils formed.[25,26] We reconfirmed these observations under the conditions used in this work; showing that $A\beta^*_{16-22}$ aggregates to yield morphologically similar fibrils to those observed for $A\beta_{16-22}$ (Figure S1).

3.3 | Analysis of cross-linked products

Cross-linking studies focused on homomeric assembly reactions of $A\beta^*_{16-22}$, that is, every peptide in the sample contained a TFMD group at position Phe20. On photolysis, (TFMD)Phe produces a highly reactive carbene which can insert rapidly and indiscriminately into proximal bonds to form a permanent covalent link.[28,35] As we have shown previously, such cross-linking approaches can yield information on noncovalent organization in self-assembled structures.[26,27] Figures S1b and c show the ion mobility spectrometry coupled to conventional mass spectrometry (IMS-MS) analyses of the PIC experiment performed on $A\beta^*_{16-22}$ after 2 weeks incubation at which time (Figure S1C) fibrils are formed. The resulting mass spectrum
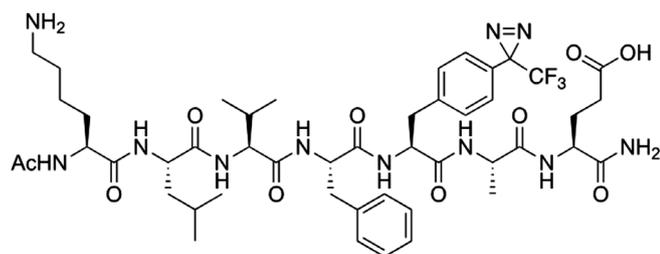
identified five major species as photolysis products (Figure S1c). Importantly, the IMS function on the mass spectrometer can provide additional information as it facilitates separation of ions with similar m/z ratios; cross-linked monomer, dimer and small amounts of trimer could be observed within the sample, in agreement with our previously published studies (Figure S1B).[26,27]

Tandem MS/MS sequencing fragments a peptide along its amide backbone, producing a variety of different fragment ions.[36-39] MS/MS analyses of cross-linked peptides allow the site(s) of crosslinking to be identified. While the peptide backbone experiences fragmentation, inter- and intramolecular crosslinks do not, and so the covalent connectivity between cross-linked peptide products is preserved and their location can be established from the fragmentation pattern. Consistent with our previous studies,[26,27] the salient conclusions of this analysis are that PIC of the $A\beta^*_{16-22}$ fibrils (Figure 3a) results in formation of intramolecular cross-links between Phe20 and Glu22, together with intermolecular cross-links between Phe20 and Lys16. These data are consistent with an assembly whereby noncovalent interactions organize peptide monomers as in-register anti-parallel β-strands in $A\beta_{16-22}$ fibrils (according to definitions described by Eisenberg and Sawaya[40]), in agreement with our earlier studies.[26,27] In such an arrangement, Phe20 is directly opposite Val18 on the adjacent strand with Lys16 diagonal to Phe20 (Figure 3b). However, rotation about the α-β bond allows side chains to adopt a range of orientations, and can be easily visualized in the structure of a related peptide Lys-Val-Leu-Phe-Phe-Ala (PDB ID: 2AYA)[41] whereby the corresponding Phe and Lys side-chains are in mutual proximity and would be expected to cross-link more easily. Such a relationship would not be possible for alternate configurations (see Figure 3c for antiparallel in-register and Supporting Information for further alternatives). Moreover subtle differences in reactivity preference of the carbene arising from diazirine photolysis could also lead to preferential reaction with Lys16 rather than Val18.

3.4 | $A\beta_{16-22}$ forms anti-parallel, in-register β-sheets in early protein assemblies

The mass spectrum of cross-linked products from $A\beta^*_{16-22}$ assembly taken at different time points (5 min, 1 hr, 24 hr, and 2 weeks) is shown in Figure 4. Intermolecular cross-links can be seen at all time points, with the intensity (relative to the H_2O quenched $A\beta_{16-22}$) increasing as time progresses. This could be attributed to an increase in the amount of fibrils formed as the incubation time is increased, or the bundling of the $A\beta_{16-22}$ fibrils after aggregation is complete. Both would increase the concentration of "dry interfaces" from which H_2O is excluded, allowing the carbene to react with peptide side-chains, rather than being quenched with H_2O to form a hydroxyl group.[35] At each time point, both dominant intermolecular cross-link peaks (i.e., m/z 998.58 and 983.50) were isolated and sequenced by MS/MS. The results from sequencing the peak at m/z 988.58 (Figure 5) are consistent with those established from sequencing of the disaggregated fibrils after 2 weeks, that is, they indicate the presence of β-sheet structure in which monomers are organized as in

FIGURE 2 The molecular structure of $A\beta^*_{16-22}$
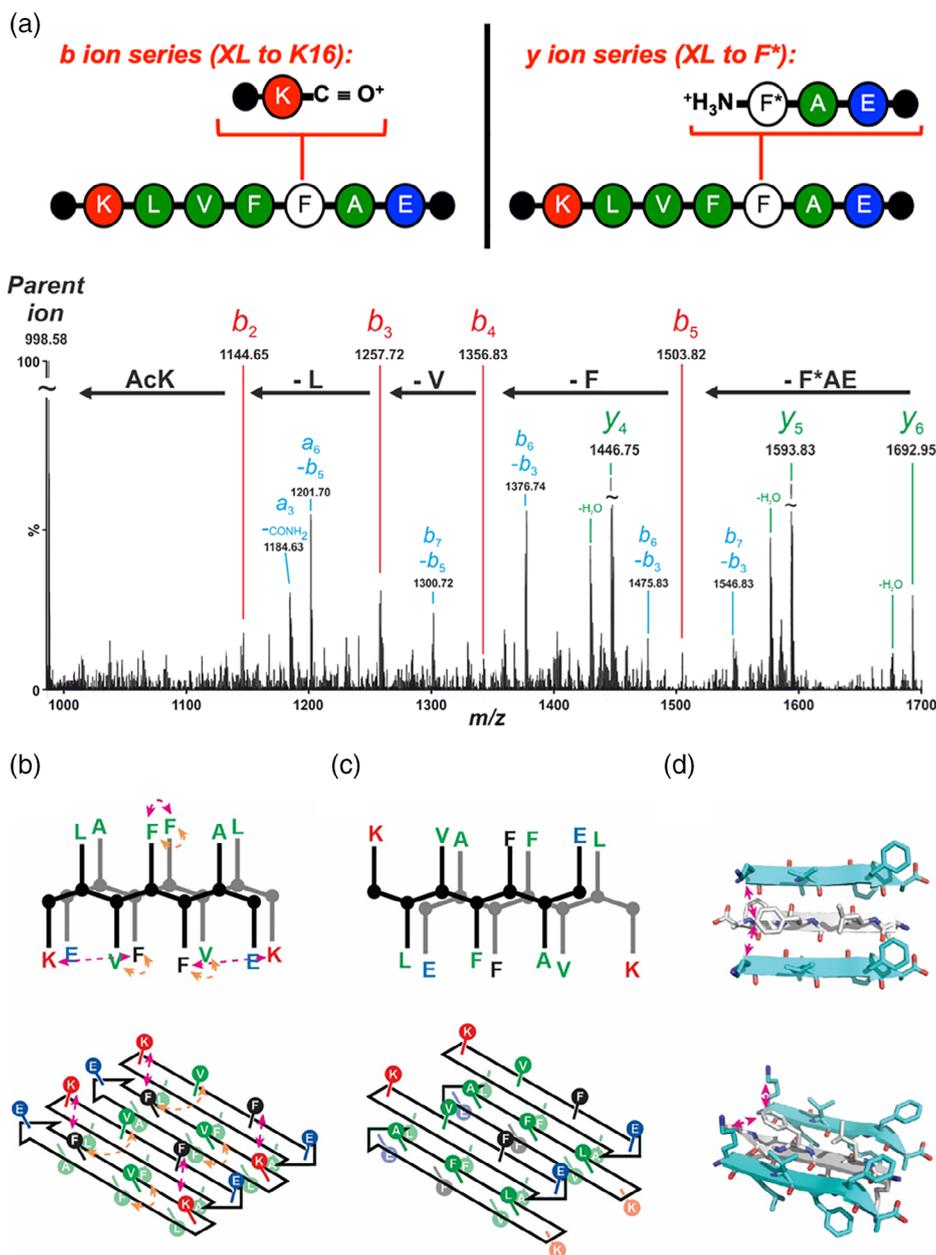
FIGURE 3 Aβ*$_{16-22}$ forms antiparallel, in-register β-sheets after 2 weeks incubation time. (a) The fully assigned tandem MS/MS spectrum for the peak at m/z 988.58 (2$^+$; mass 1975.16 Da) contains b ions (red, e.g., at 1503.82 corresponding to the loss of F*AE i.e., TFMD-Phe-Ala-Glu), y ions (green, e.g., at 1692.95 corresponding to the lost of Lys-Leu) and double fragmentation products (blue). The two major fragmentation series (b and y ion) located the cross-link position to Lys16 and Phe20 on the acceptor chain respectively. Both of these cross-link patterns are consistent with an antiparallel in-register β-strand assembly. Cartoon schematic (b) for in-register antiparallel and (c) out-of-register antiparallel organization of strands (top shows side, bottom shows angle from above, pink arrows illustrate crosslinks observed in this or earlier studies, salmon arrows show contacts observed from MD simulations [see later]). (d) Structure of Lys-Val-Leu-Phe-Phe-Ala depicting in-register antiparallel organization of strands highlighting proximity of Phe and Lys (pink arrows) between adjacent strands (alternate strands shown in cyan and top shows above, bottom shows angle from above) [Color figure can be viewed at wileyonlinelibrary.com]

register anti-parallel β-strands. The absence of any other cross-links can be interpreted as follows: (a) Aβ$_{16-22}$ assembly proceeds through oligomers in which monomers are aligned as anti-parallel, in-register β-strands akin to those in the fibrillar state or (b) cross-linking reports only on oligomeric and fibrillar assemblies where monomers are assembled as anti-parallel in register β-strands, with the remaining species being either too heterogeneous to be sufficiently populated for detection by mass-spectrometry or too disordered to generate cross-links other than to water and buffer components.

3.5 | Large scale DMD simulations of Aβ$_{16-22}$ assembly

To help determine the nature of oligomers formed during Aβ$_{16-22}$ assembly, DMD and PRIME20 simulations were performed to

visualize the transitions that occur during the self-assembly process. The simulations were conducted as described in Section 2 and a series of simulation snapshots were taken at different time points, as shown in Figure 6. After 652 ns of simulation time, most peptides were still in a random coil conformation with some disordered aggregates and small amounts of ordered oligomers present. As the simulation progressed (1,278 ns), the formation of an anti-parallel, in-register oligomer could be clearly seen, as well as a small amount of disordered aggregates. This is in excellent agreement with the structures observed by TEM at early time points (~5 min) where both fibrils and amorphous aggregates are present. At later time points (2,519 and 6,283 ns), most peptides were in ordered aggregates with anti-parallel, in-register structures dominating. A single, four-layered β-sheet structure was present at the simulation end point (12,661 ns). Again, these results are in close agreement with the experimental data, in which both ordered fibrils and amorphous aggregates were observed at early

FIGURE 4 At all time points analyzed Aβ*$_{16-22}$ forms both intra- and intermolecular peptide cross-links. Products from the reaction between the carbene and H_2O are labeled in blue and peptide cross-links are labeled in black [Color figure can be viewed at wileyonlinelibrary.com]
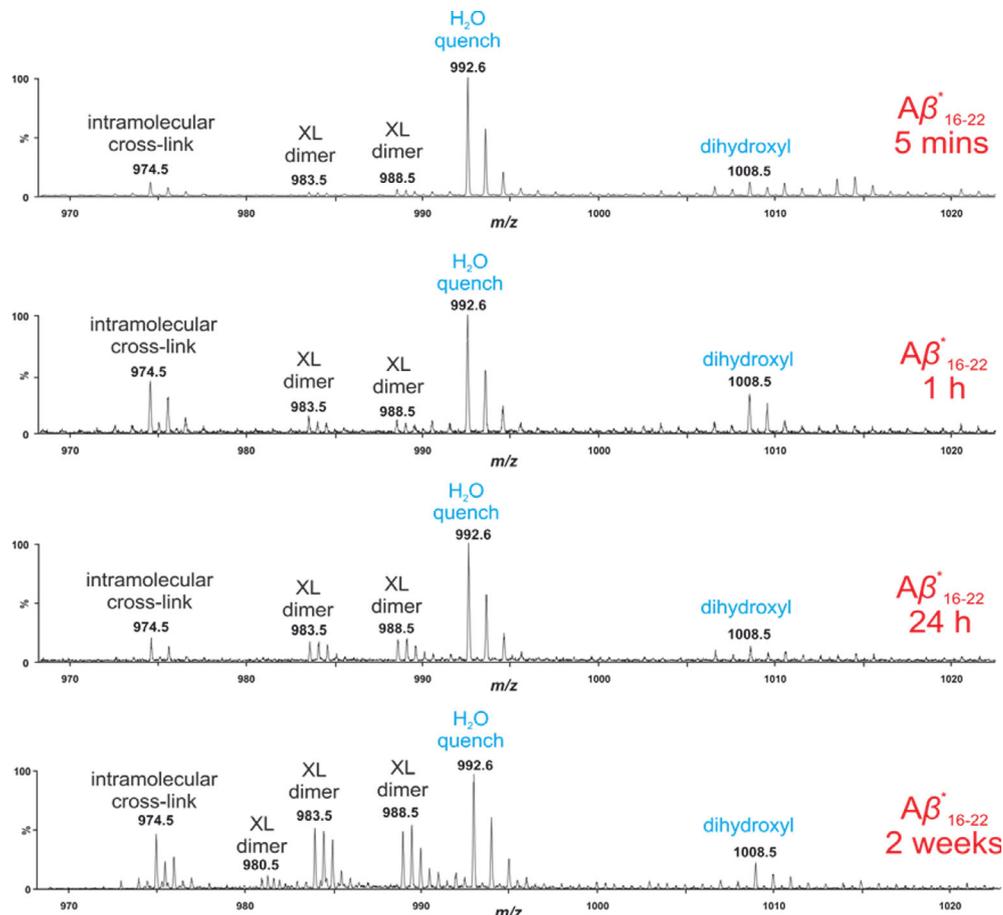

time points (presumably after a hydrophobic collapse of the peptides upon solvation), prior to the disappearance of the amorphous aggregates and continued formation of fibrils.

The kinetics of Aβ$_{16-22}$ aggregation can be measured in the simulation by calculating the percentage of residues that are in a β-sheet conformation at different simulation times. Figure 7 demonstrates that, in agreement with the fluorescence quenching data, aggregation proceeds via a rapid increase in β-sheet content, as measured by the decrease in the system potential energy (from 0 to 50% in the first 4,000 ns) followed by a slower second phase (4,000–12,000 ns). The TEM time course (Figure 1) and the simulation snapshots (Figure 6; i.e., hydrophobic collapse and the presence of small amounts of fibrils at early time points followed by a transition to/continued fibril formation) are concordant, as is the two phase kinetics observed in both the fluorescence quenching and the simulations.

3.6 | Side-chain contacts formed during DMD simulations of Aβ$_{16-22}$ self-assembly

The DMD/PRIME20 simulations approach taken in this study can also be used to assess the distance between the beads which represent specific side-chains beads as the simulation progresses and may be able to identify structures that cannot be resolved in the PIC experiment. To do this, the nearest interpeptide sidechain contacts for all

Phe19 and Phe20 residues in the system are calculated and shown in Figure 8. Figure S2 shows a schematic illustrating the simplest anti-parallel/ parallel in-register/out-of-register potential arrangements that can be envisioned. At the simulation end point, both Phe19 and Phe20 make the most contacts with the residues that are directly opposite their side-chains in an anti-parallel, in-register orientation (Phe19 and Val18, respectively, see Figure 3). Although in isolation the Phe19-Phe19 contact observed in the simulation would be consistent with both parallel and anti-parallel orientations of monomers as in-register β-strands, in combination with the Phe20 data, the identified contacts are most consistent with an anti-parallel, in-register orientation as the dominant mode of interaction. The discrepancy between these MD simulations and the PIC experiments where a cross-link between Lys16 and Phe20 dominates is reconciled by the fact that PRIME 20 models amino acid side chains as spheres, thus such rotational preferences are not resolved and, instead, a simple distance relationship is observed. Within the data, three distinct phases are observed, which occur on the 0–2,000, 2,000–4,000, and 4,000–12,000 ns timescales. As can be seen in Figure 8a, the second most frequent contact that residue Phe19 makes during the simulation is with Val18 (curve labeled Phe19-Val18). This contact increased steadily until ~2,000 ns, at which point no further increase occurred. Contact between Phe19 and Val18 would be possible in a parallel out-of-register conformation (Figure S2). When analyzing the contacts that Phe20 forms during this initial period (Figure 8b), two significant
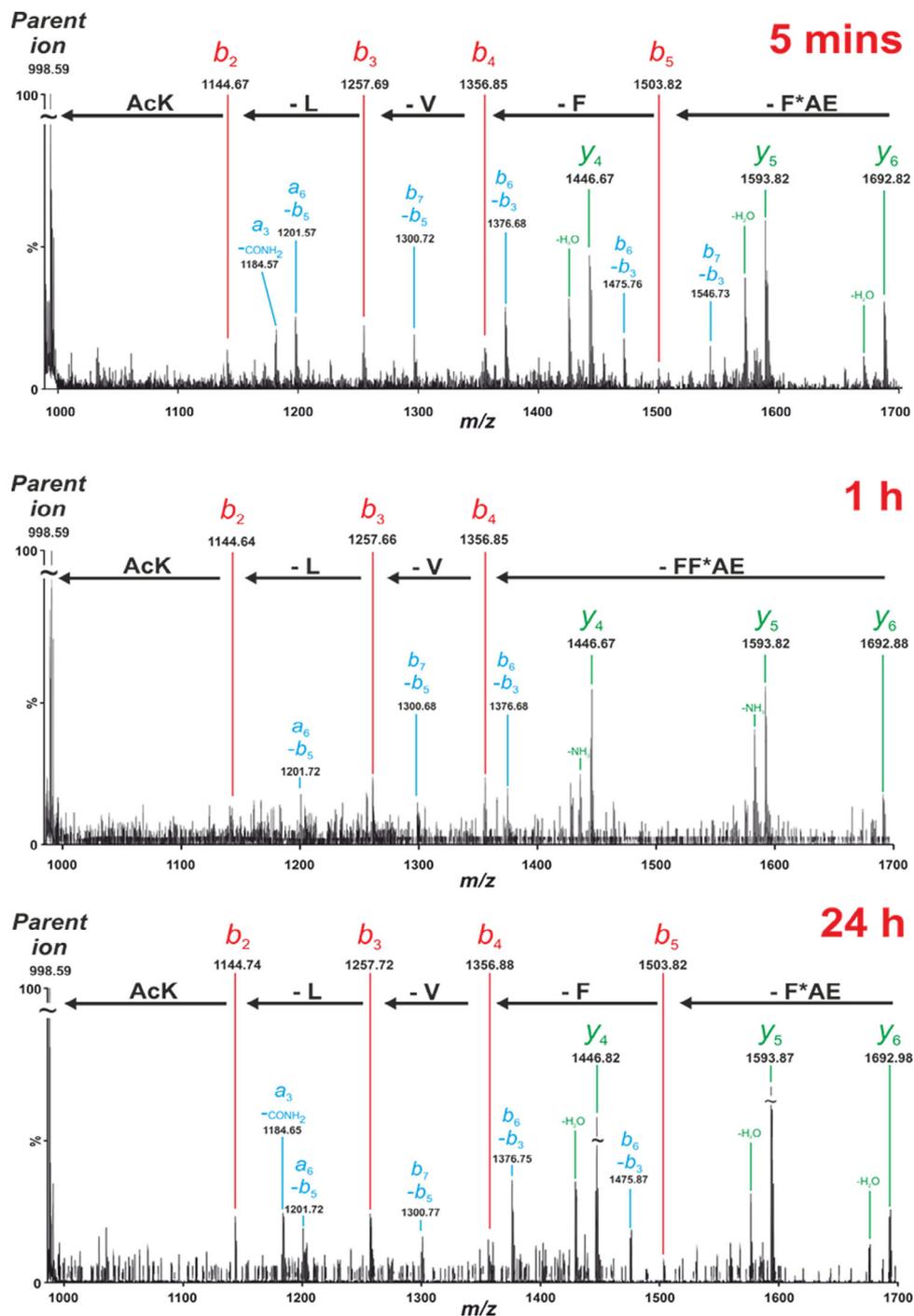
FIGURE 5 Annotated tandem MS/MS spectra demonstrating that at all time points analyzed $A\beta^*_{16-22}$ forms anti-parallel, in-register β-strands. In the spectra, *b* ions are highlighted in red, *y* ions in green and any double fragmentation products in blue [Color figure can be viewed at wileyonlinelibrary.com]
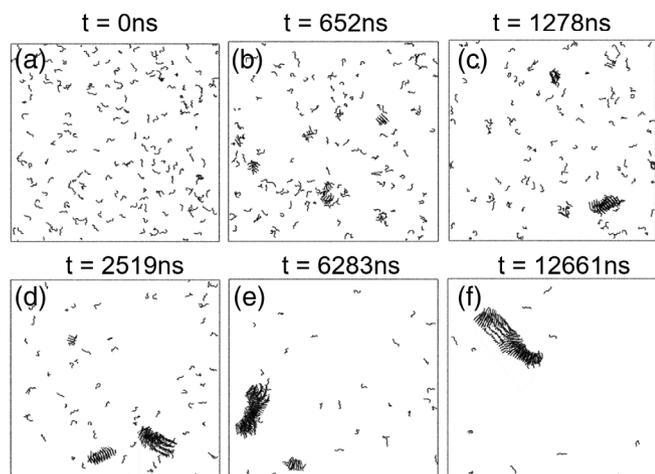
contacts (other than the dominant Phe20-Val18 contact) are observed: Phe20-Leu17 and Phe20-Phe20. Phe20-Leu17 interaction would not occur for any of the simplest monomer organizations; this contact again continued to increase in population until ~2,000 ns at which time the number of contacts remained stable for the rest of the simulation. The Phe20-Phe20 contact, possible in a parallel-in-register alignment (Figure S2), increased at a slightly slower rate than the Phe20-Leu17 contact in the first phase. However, rather than stopping at 2000 ns, it continued to increase until it plateaued at ~4,000 ns. Taken together, the results suggest that

as the simulation progresses, an anti-parallel in-register β-sheet forms, while a plethora of alternative structures are also present including disordered aggregates (particularly at early time points), where a heterogeneous distribution of sidechain contacts would be expected. After 2000 ns, however, the anti-parallel, in-register alignment starts to dominate, while the contacts for other alignments plateau, indicating that these structures no longer grow, and may interconvert to the in-register alignment, in agreement with the experimental observations made by Lynn and co-workers.[13] These series of simulations demonstrate the power of combining

simulations and experimental data to gain a fuller picture of peptide self-assembly at an atomistic level.
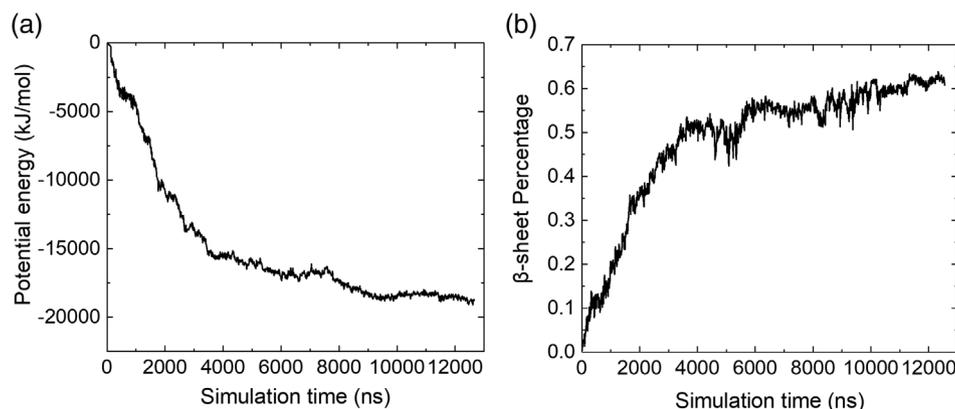
3.7 | Proposed mechanism of aggregation and comparison with previously proposed Aβ₁₆₋₂₂ aggregation mechanisms

According to the experimental data, the following mechanism for Aβ₁₆₋₂₂ self-assembly is proposed (Figure 9): peptides aggregate rapidly, forming both fibrils and small amounts of amorphous aggregates (the initial decrease in fluorescence, $\sim$ 5 min). These amorphous aggregates then form fibrils, with most of the self-assembly reaction completed within 1–2 hr (as evidenced by the plateau in the fluorescence quenching data). The fibrils formed at these time points tend to be isolated and unbundled. As the self-assembly reaction continues, the fibrils start to bundle together and coalesce, forming dense mats of fibril structures (after 2 weeks). These large mats (partly) exclude H_2O, forming a series of dry interfaces, in turn reducing the opportunity for H_2O to quench the carbene and promoting the formation of interpeptide cross-links.
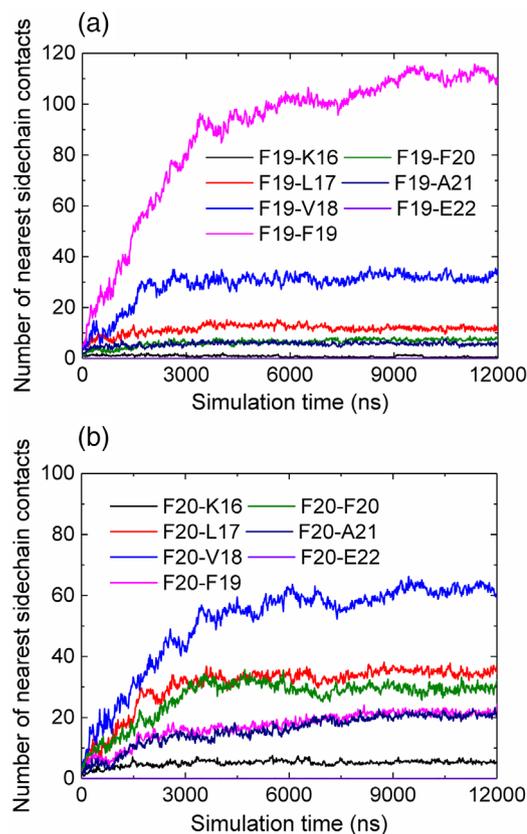
Lynn and co-workers previously observed a transition from out-of-register, anti-parallel β-sheets before Aβ₁₆₋₂₂ assembles into its final in-register alignment.[13] No such transition was discernable in our cross-linking data. There could be a number of reasons for this:

1. The out-of-register alignment may be lowly populated compared with the in-register alignment and as such may not be captured by the cross-linking experiments at early time points; this is supported by our simulations.

FIGURE 8 Analysis of the closest interpeptide sidechain contacts formed by F19 (a) and F20 (b) with the other residues of Aβ₁₆₋₂₂ in the system as a function of simulation time [Color figure can be viewed at wileyonlinelibrary.com]

FIGURE 6 DMD simulation of 192 Aβ₁₆₋₂₂ peptides at T^* = 0.193 (T = 326 K). Snapshots of the system were taken at 0 ns (a), 652 ns (b), 1,278 ns (c), 2,519 ns (d), 6,283 ns (e) and 12,661 ns (f)

FIGURE 7 (a) System potential energy profile versus time and (b) Percentage of residues that adopt β-sheet structures in the system versus time

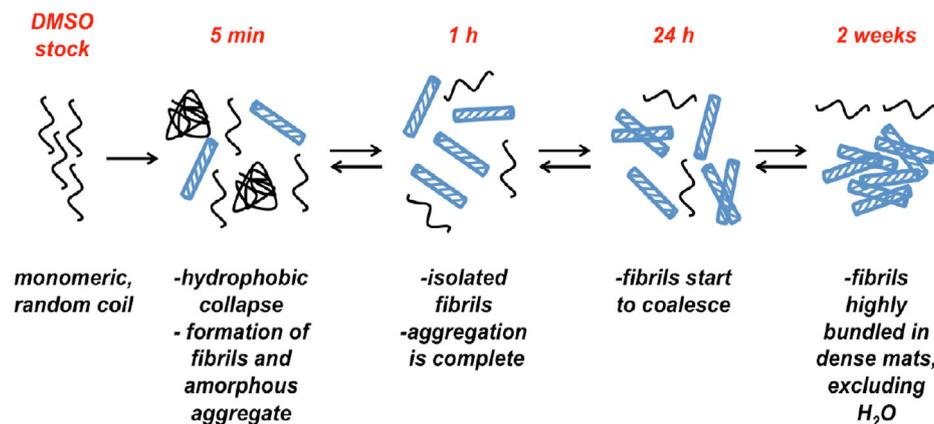**FIGURE 9** The proposed mechanism for Aβ$_{16-22}$ self-assembly [Color figure can be viewed at wileyonlinelibrary.com]

2. The experimental conditions in this study and the previously reported work of Lynn and co-workers were different. The prior publication focused on self-assembly carried out in H$_2$O and 40% MeCN with no added salt (i.e., at very low ionic strength), and at higher Aβ$_{16-22}$ concentration (1.3 mM)[42] whereas in the present study self-assembly was carried out in 100 mM ammonium bicarbonate buffer with a peptide concentration of 40 μM. This could cause the out-of-register alignment to be disfavored and therefore bypassed, or to be present only transiently prior to the time-point at which useful cross-linking data could be obtained (i.e., 5 min).

4 | CONCLUSION

In this work, Aβ$_{16-22}$, a TAMRA-labeled Aβ$_{16-22}$ peptide variant and an Aβ*$_{16-22}$ peptide variant were synthesized and used in fluorescence quenching and PIC assays to demonstrate that Aβ$_{16-22}$ aggregates in two distinct phases. In the first phase, the peptides self-assemble into β-sheet assemblies causing the fluorescence intensity to decrease rapidly (∼10 min). This is followed by a slower, second phase that plateaus after 1–2 hr. A TEM time course confirmed that fibrils are present after 5 min. To characterize the structures at a number of different time points, the PIC reagent Fmoc-TFMD-Phe was synthesized and incorporated into Aβ*$_{16-22}$. PIC with ESI-IMS-MS/MS at different time points confirmed that Aβ*$_{16-22}$ forms assemblies in which monomers are organized as anti-parallel, in-register β-strands at all time points. These experimental results were then compared with a series of detailed DMD simulations that are in agreement with the experimental data and allow a molecular mechanism to be proposed for Aβ$_{16-22}$ assembly under the conditions used in this study, where the dominant pathways involve oligomers where monomers are organized into anti-parallel, in-register β-strands. The DMD results also highlight the presence of intermediary structures that could not be trapped by PIC. Together, the results demonstrate that the combination of crosslinking and MD represents a powerful toolkit with which to visualize the mechanisms of peptide aggregation in molecular and kinetic detail. Such approaches provide proof-of-concept for the application of these methods to the study of: (i) disease relevant amyloidogenic peptides (e.g., in Alzheimer's and Parkinson's disease) and (ii) peptide materials.

AUTHOR CONTRIBUTIONS

Samuel Bunce: Conceptualization; data curation; formal analysis; investigation; methodology; resources; validation; visualization; writing-original draft. **Yiming Wang:** Data curation; formal analysis; investigation; methodology; writing-original draft; writing-review and editing. **Sheena Radford:** Funding acquisition; supervision; writing-review and editing. **Andrew Wilson:** Funding acquisition; project administration; resources; supervision; validation; visualization; writing-original draft; writing-review and editing. **Carol Hall:** Funding acquisition; investigation; project administration; supervision; writing-review and editing.

DATA AVAILABILITY STATEMENT

Data in addition to those in the supplementary material are available on request.

NOTATION

Aβ	amyloid β
DMD	discontinuous molecular dynamics

ESI- electrospray ionization ion-mobility spectrometry mass-

IMS-MS spectrometry

PIC photo-induced crosslinking

TEM transmission electron microscopy

ORCID

Yiming Wang https://orcid.org/0000-0003-3657-6100

Andrew J. Wilson https://orcid.org/0000-0001-9852-6366

REFERENCES

1. Iadanza MG, Jackson MP, Hewitt EW, Ranson NA, Radford SE. A new era for understanding amyloid structures and disease. *Nat Rev Mol Cell Biol*. 2018;19:755-773.

2. Adler-Abramovich L, Gazit E. The physical properties of supramolecular peptide assemblies: from building block association to technological applications. *Chem Soc Rev*. 2014;43:6881-6893.

3. Törnquist M, Michaels TC, Sanagavarapu K, et al. Secondary nucleation in amyloid formation. *Chem Commun*. 2018;54:8667-8684.

4. Wang J, Liu K, Xing R, Yan X. Peptide self-assembly: thermodynamics and kinetics. *Chem Soc Rev*. 2016;45:5589-5604.

5. Balbach JJ, Ishii Y, Antzutkin ON, et al. Amyloid fibril formation by Aβ16-22, a seven-residue fragment of the Alzheimer's β-amyloid peptide, and structural characterization by solid state NMR. *Biochemistry*. 2000;39:13748-13759.

6. Balbirnie M, Grothe R, Eisenberg DS. An amyloid-forming peptide from the yeast prion Sup35 reveals a dehydrated β-sheet structure for amyloid. *Proc Natl Acad Sci U S A*. 2001;98:2375-2380.

7. Nelson R, Sawaya MR, Balbirnie M, et al. Structure of the cross-β spine of amyloid-like fibrils. *Nature*. 2005;435:773-778.

8. Sawaya MR, Sambashivan S, Nelson R, et al. Atomic structures of amyloid cross-β spines reveal varied steric zippers. *Nature*. 2007;447:453-457.

9. Hilbich C, Kisters-woike B, Reed J, Masters CL, Beyreuther K. Aggregation and secondary structure of synthetic amyloid βA4 peptides of Alzheimer's disease. *J Mol Biol*. 1992;218:460-473.

10. Bitan G, Vollers SS, Teplow DB. Elucidation of primary structure elements controlling early amyloid β-protein oligomerization. *J Biol Chem*. 2003;278:34882-34889.

11. Wurth C, Guimard NK, Hecht MH. Mutations that reduce aggregation of the Alzheimer's Aβ42 peptide: an unbiased search for the sequence determinants of Aβ amyloidogenesis. *J Mol Biol*. 2002;319:1279-1290.

12. Lu K, Jacob J, Thiyagarajan P, Conticello VP, Lynn DG. Exploiting amyloid fibril lamination for nanotube self-assembly. *J Am Chem Soc*. 2003;125:6391-6393.

13. Hsieh MC, Liang C, Mehta AK, Lynn DG, Grover MA. Multistep conformation selection in amyloid assembly. *J Am Chem Soc*. 2017;139:17007-17010.

14. Sipe JD, Benson MD, Buxbaum JN, et al. Amyloid fibril proteins and amyloidosis: chemical identification and clinical classification International Society of Amyloidosis 2016 nomenclature guidelines. *Amyloid*. 2016;23:209-213.

15. Eisenberg DS, Jucker M. The amyloid state of proteins in human diseases. *Cell*. 2012;148:1188-1203.

16. Petty SA, Decatur SM. Experimental evidence for the reorganization of β-strands within aggregates of the Aβ (16−22) peptide. *J Am Chem Soc*. 2005;127:13488-13489.

17. Childers WS, Anthony NR, Mehta AK, Berland KM, Lynn DG. Phase networks of cross-β peptide assemblies. *Langmuir*. 2012;28:6386-6395.

18. Anthony NR, Mehta AK, Lynn DG, Berland KM. Mapping amyloid-β(16-22) nucleation pathways using fluorescence lifetime imaging microscopy. *Soft Matter*. 2014;10:4162-4172.

19. Senguen FT, Lee NR, Gu X, et al. Probing aromatic, hydrophobic, and steric effects on the self-assembly of an amyloid-β fragment peptide. *Mol BioSyst*. 2011;7:486-496.

20. Klimov DK, Thirumalai D. Dissecting the assembly of Aβ16-22 amyloid peptides into antiparallel β sheets. *Structure*. 2003;11:295-307.

21. Santini S, Wei G, Mousseau N, Derreumaux P. Pathway complexity of Alzheimer's β-amyloid Aβ16-22 peptide assembly. *Structure*. 2004;12:1245-1255.

22. Röhrig UF, Laio A, Tantalo N, Parrinello M, Petronzio R. Stability and structure of oligomers of the Alzheimer peptide Aβ16−22: from the dimer to the 32-mer. *Biophys J*. 2006;91:3217-3229.

23. Cheon M, Chang I, Hall CK. Spontaneous formation of twisted Aβ16-22 fibrils in large-scale molecular-dynamics simulations. *Biophys J*. 2011;101:2493-2501.

24. Wang Y, Bunce SJ, Radford SE, Wilson AJ, Auer S, Hall CK. Thermodynamic phase diagram of amyloid-β (16−22) peptide. *Proc Natl Acad Sci U S A*. 2019;116:2091-2096.

25. Bunce SJ, Wang Y, Stewart KL, et al. Molecular insights into the surface catalysed secondary nucleation of amyloid-β (Aβ40) by the peptide fragment Aβ16-22. *Sci Adv*. 2019;5:eaav8216.

26. Preston GW, Radford SE, Ashcroft AE, Wilson AJ. Covalent cross-linking within supramolecular peptide structures. *Anal Chem*. 2012;84:6790-6797.

27. Preston GW, Radford SE, Ashcroft AE, Wilson AJ. Analysis of amyloid nanostructures using photo-cross-linking: in situ comparison of three widely used photo-cross-linkers. *ACS Chem Biol*. 2014;9:761-768.

28. Horne JE, Walko M, Calabrese AN, et al. Rapid mapping of protein interactions using tag-transfer photocrosslinkers. *Angew Chem Int Ed*. 2018;57:16688-16692.

29. Smith DP, Knapman TW, Campuzano I, et al. Deciphering drift time measurements from travelling wave ion mobility spectrometry-mass spectrometry studies. *Euro J Mass Spectrom*. 2009;15:113-130.

30. Valentine SJ, Counterman AE, Clemmer DE. A database of 660 peptide ion cross sections: use of intrinsic size parameters for bona fide predictions of cross sections. *J Am Soc Mass Spectrom*. 1999;10:1188-1211.

31. Cheon M, Chang I, Hall CK. Extending the PRIME model for protein aggregation to all 20 amino acids. *Proteins: Struct, Func Bioinf*. 2010;78:2950-2960.

32. Alder BJ, Wainwright TE. Studies in molecular dynamics. I. General method. *J Chem Phys*. 1959;31:459-466.

33. Wang Y, Shao Q, Hall CK. N-terminal prion protein peptides (PrP [120-144]) form parallel in-register β-sheets via multiple nucleation-dependent pathways *J. Biol. Chem*. 2016;291: 22093-22105. *Correction*. 2017;292:20655-20655.

34. Garai K, Frieden C. Quantitative analysis of the time course of Aβ oligomerization and subsequent growth steps using tetramethylrhodamine-labeled Aβ. *Proc Natl Acad Sci U S A*. 2013;110:3321-3326.

35. Preston GW, Wilson AJ. Photo-induced covalent cross-linking for the analysis of biomolecular interactions. *Chem Soc Rev*. 2013;42:3289-3301.

36. Biemann K. Mass spectrometry of peptides and proteins. *Annu Rev Biochem*. 1992;61:977-1010.

37. Uetrecht C, Rose RJ, van Duijn E, Lorenzen K, Heck AJ. Ion mobility mass spectrometry of proteins and protein assemblies. *Chem Soc Rev*. 2010;39:1633-1655.

38. Paizs B, Suhai S. Fragmentation pathways of protonated peptides. *Mass Spectrometry Reviews, Mass Spectrom Rev*. 2005;24:508-548.

39. Medzihradszky KF, Chalkley RJ. Lessons in de novo peptide sequencing by tandem mass spectrometry. *Mass Spectrom Rev*. 2015;34:43-63.

40. Eisenberg DS, Sawaya MR. Structural studies of amyloid proteins at the molecular level. *Annu Rev Biochem*. 2017;86:69-95.

41. Colletier JP, Laganowsky A, Landau M, et al. Molecular basis for amyloid-β polymorphism. *Proc Natl Acad Sci U S A*. 2011;108:16938-16943.

42. Mehta AK, Lu K, Childers WS, et al. Facial symmetry in protein self-assembly. *J Am Chem Soc*. 2008;130:9829-9835.

SUPPORTING INFORMATION

Additional supporting information may be found online in the Supporting Information section at the end of this article.